Energy threshold for the creation of nanodots on $SrTiO_3$ by swift heavy ions

2010 New J. Phys. 12 043009

(http://iopscience.iop.org/1367-2630/12/4/043009)

New Journal of Physics
The open-access journal for physics

Energy threshold for the creation of nanodots on $SrTiO_3$ by swift heavy ions

Marko Karlušić[1], Sevilay Akcöltekin[2], Orkhan Osmani[2,3], Isabelle Monnet[4], Henning Lebius[4], Milko Jakšić[1] and Marika Schleberger[2,5]

[1] Institut Ruder Bošković, PO Box 180, 10002 Zagreb, Croatia
[2] Fakultät für Physik, CeNIDE, Universität Duisburg-Essen, 47048 Duisburg, Germany
[3] Physics Department and Research Center OPTIMAS, University of Kaiserslautern, 67663 Kaiserslautern, Germany
[4] CIMAP (CEA-CNRS-ENSICAEN-UCBN), 14070 Caen Cedex 5, France
E-mail: marika.schleberger@uni-due.de

New Journal of Physics **12** (2010) 043009 (10pp)
Received 6 November 2009
Published 1 April 2010
Online at http://www.njp.org/
doi:10.1088/1367-2630/12/4/043009

Abstract. We present experimental and theoretical data on the threshold behaviour of nanodot creation with swift heavy ions. A model calculation based on a two-temperature model that takes into account the spatially resolved electron density gives a threshold of 12 keV nm^{-1} below which the energy density at the end of the track is no longer high enough to melt the material. In the corresponding experiments, we irradiated $SrTiO_3$ surfaces under grazing incidence with swift heavy ions. The resulting chains of nanodots were analysed by atomic force microscopy (AFM). In addition, some samples of $SrTiO_3$ irradiated under normal incidence were analysed by transmission electron microscopy (TEM). Both experiments showed two thresholds, which were connected with the appearance of tracks and the creation of fully developed tracks. The threshold values were similar for surface and bulk tracks, suggesting that the same processes occur at both glancing and normal incidence.

[5] Author to whom any correspondence should be addressed.

Contents

1. Introduction

The irradiation of solid matter using heavy ions with energies in the MeV range has long been known to result in structural modifications such as stoichiometric or morphological changes, amorphization of the bulk and the creation of hillocks as well as chains of hillocks on the surface [1–5]. In this energy range, the modification of the material is not due to direct collisions of the projectile ion with the target atoms (nuclear stopping power regime) but rather to a very intense interaction of the projectile with the electronic system of the target (electronic stopping power regime). How this electronic excitation is transformed into material modifications depends very much on the physical properties of the target material itself. Most insulating materials exhibit nanosized hillocks at the impact zone of the ion when irradiated normal to the surface. This effect has been evidenced and studied in detail for many years (e.g. [6–8]) but is still not fully understood.

A rather successful approach for describing the conversion of an electronic excitation into a heated lattice is based on a two-temperature model (TTM) and requires solving the coupled differential equations for the electron and phonon temperatures [9]. The model has been used to explain the track radii in various materials created by irradiation perpendicular to the surface under the condition that the electron–phonon coupling constant g is a fitting parameter.

Recently, the TTM has been modified to include the spatially resolved electron density instead of a homogeneous free electron gas [5], which is important if the irradiation takes place under glancing angles. In this case, a single ion is able to create a chain of hillocks along its otherwise latent track within the bulk. According to the model, the chains occur due to the non-homogeneous nature of the electron density. Every time the projectile travels through a region with a high density, the energy loss is sufficiently high to feed energy into the electronic system. This energy is transferred into the phonon system, and a local melting occurs, which finally results in a nanodot on the surface. Because the electron density reflects the periodicity of the crystal, the nanodots appear with a certain periodicity on the surface.

So far, these chains of hillocks have always been produced with ions experiencing a stopping power of about 20 keV nm^{-1}, and nothing is known about the morphology at lower stopping powers. The aim of this paper is to study ion-induced nanodot chains in $SrTiO_3$ as a function of the kinetic energy of the projectile to determine a threshold value for the stopping power. In addition, we wish to show that the recently presented theoretical approach can be applied to predict a threshold value that is in agreement with experimental data.

This paper is organized as follows. We first present experimental data from two different methods to determine the threshold energy for the production of nanodots. Next, in section 2.1, we discuss the use of atomic force microscopy (AFM) to determine the minimum stopping power required to create a chain of nanodots on the surface. As we normally treat the surface chains as *tracks on the surface*, it is interesting to compare the two manifestations of a swift-ion passage: surface chains and tracks in the bulk. Therefore, in section 2.2, we present the results obtained with transmission electron microscopy (TEM) to determine the stopping power required for amorphization. We then derive a value for the threshold from theory and compare the experimental data with our theoretical predictions.

2. Experimental determination of threshold values

2.1. Grazing incidence

Single crystal samples of $SrTiO_3(100)$ (Crystec, Berlin, and Kelpin, Neuhausen) were irradiated, at room temperature without prior surface treatment, at the 6.0 MV Tandem Van de Graaff accelerator of Institut Ruder Bošković [10]. The irradiations were performed using I ions with different kinetic energies, resulting in different stopping powers (calculated with SRIM [11]): 6.5, 13, 18, 23 and 28 MeV, yielding 2.9, 5.3, 7.2, 9.0 and 10.5 keV nm^{-1}, respectively. The angle of incidence with respect to the surface was fixed at $\phi = 1.3^\circ$. The samples were oriented along the (001) direction within a few degrees. Fluences were typically chosen to yield around 10 tracks per μm^2 on average, assuming that every ion produces one track. For lower stopping powers, higher fluences were used to compensate for a possible loss in production efficiency. Additional samples of $SrTiO_3(100)$ were irradiated under $\phi = 1^\circ$ at the IRRSUD (92 MeV Xe^{23+}, 21 keV nm^{-1}) and SME (700 MeV Xe^{23+}, 29 keV nm^{-1}) beam lines of GANIL (Caen, France). After irradiation, the samples were analysed by AFM in tapping mode under ambient conditions. Some samples were cleaned prior to AFM measurements by snow-cleaning and wiping with ethanol. By comparing chains of nanodots from irradiated samples with and without cleaning treatment, we made sure that this procedure did not affect either the shape or the height of the hillocks. All AFM images were processed with the software package WSxM [12].

The typical surface track morphology that is obtained in a glancing angle geometry if the projectile energy is high enough can be seen in figure 1(c). This $SrTiO_3$ surface was irradiated with 10.5 keV nm^{-1} ions at a glancing angle of $\phi = 1.3^\circ$. Each chain in figure 1(c) was produced by a single ion because the average number of chains ($\approx$10 per μm^2) corresponds well with the nominal fluence of 1×10^9 ions cm^{-2}. Thus, the production efficiency is close to one. The chain length is about 300 nm, and the individual hillocks within the chains are a few nanometres high. The length of the track as well as the typical separation of the dots is in good agreement with earlier experiments on a variety of materials [5, 13]; the influence of the direction of the incoming beam on the morphology has been discussed in [14, 15]. At this stopping power, the height and diameter of the dots appear to be the same as found in earlier experiments with higher stopping powers (see figures 1(d) and (e)). For a general discussion of the velocity effect in the electronic energy loss region on the measured chains of hillocks, see [16].

In figures 1(a) and (b), we show representative AFM images of samples irradiated with ions of 5.3 keV nm^{-1} and 7.2 keV nm^{-1}, respectively (the same fluence and the same angle as in figure 1(c)). The morphology is clearly different from the one shown in figure 1(c). Ions with

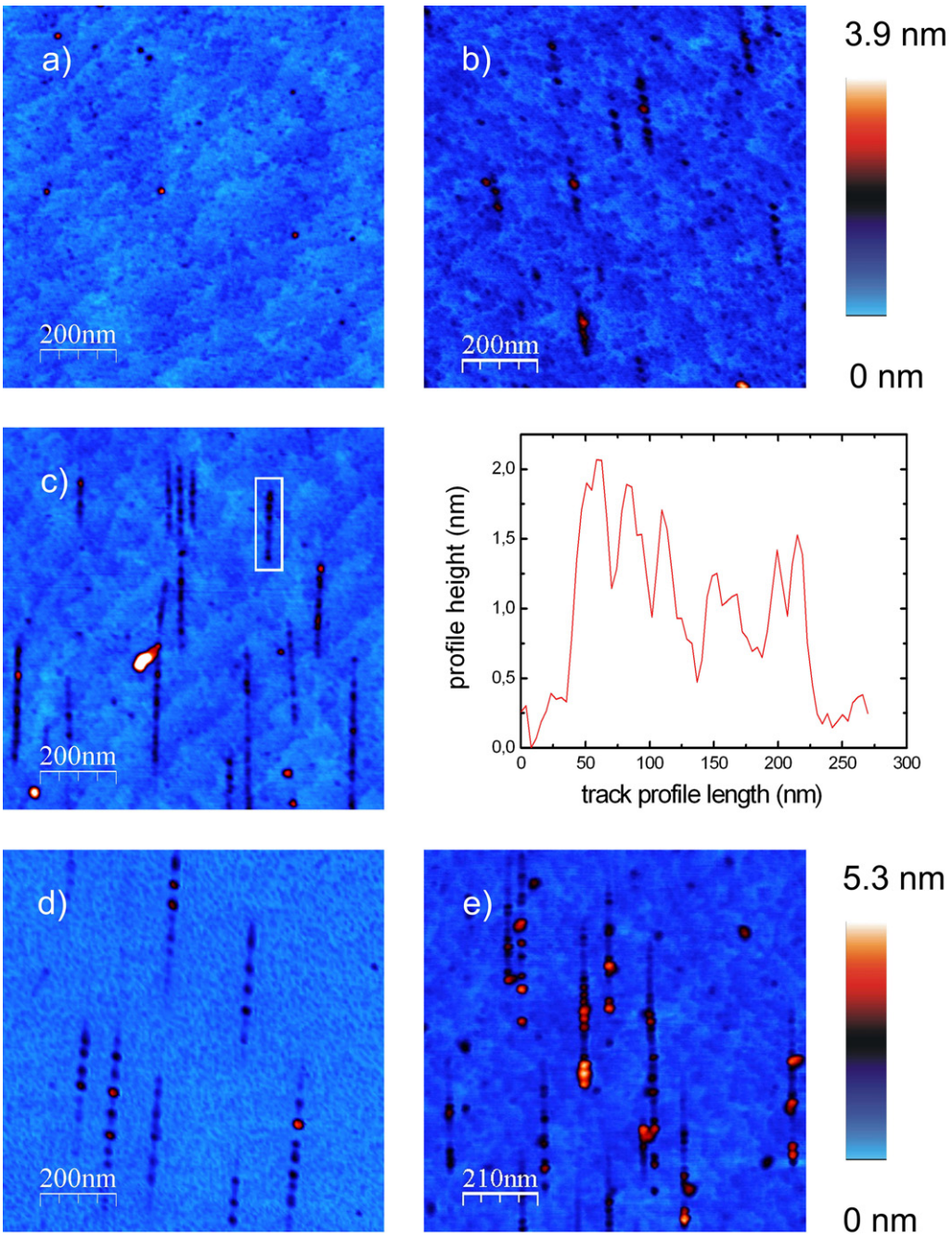

Figure 1. Topographic images of a $SrTiO_3$ surface irradiated with different energy losses under grazing incidence. Whereas I ions at $\phi = 1^\circ$ were used in (a)–(c), Xe ions at $\phi = 1^\circ$ were used in (d, e). The frame size was 1 μm × 1 μm. To enhance the contrast, false colouring was used. Electronic energy losses in the sub parts of the figure are (a) 5.3 keV nm^{-1}, (b) 7.2 keV nm^{-1}, (c) 10.5 keV nm^{-1} with a height profile of the marked track, (d) 21 keV nm^{-1} and (e) 29 keV nm^{-1}.

5.3 keV nm^{-1} (figure 1(a)) as well as with lower energy losses produce no visible chains. Chains were first detected at 7.2 keV nm^{-1} (figure 1(b)). As can be seen, the average chain length as well as the number of chains is smaller than for higher energy losses. Our statistical data were

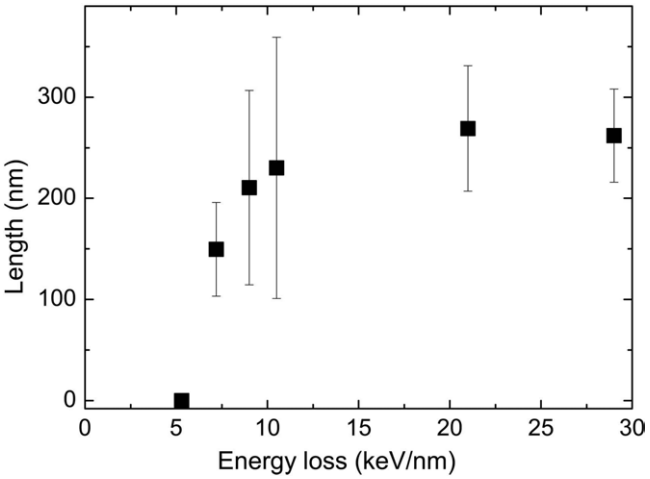

Figure 2. Chain length as a function of stopping power. The data points at 21 and 29 keV nm^{-1} are taken from samples irradiated with Xe ions under 1°. The chain length was corrected to present an incidence angle of $\phi = 1.3°$, i.e. they were divided by $\cot 1.3°/\cot 1° = 1.3$. The other data points are from irradiations with iodine ions at $\phi = 1.3°$.

not sufficient to quantitatively discuss the chain production efficiency (chains per incident ion), but we were able to study the length of the chains.

To demonstrate more clearly the evolution of chains as a function of ion energy, we have performed a statistical analysis of at least 60 chains for each kinetic energy, see figure 2. It should be noted that the error bars in the length measurement do not originate from uncertainties in the measurement itself, but from the statistical nature of the interaction process. From figure 2, we find that the minimum stopping power needed to create a chain is between 5.3 and 7.2 keV nm^{-1}. Up to a stopping power of between 10.5 and 21 keV nm^{-1}, the chain length increases with increasing kinetic energy until a constant chain length is reached. The SRIM calculations as well as our calculations in section 3 were made for Xe ions. Because iodine is right next to xenon in the periodic table, there is not much difference between these two ions with respect to the modifications they produce. Experimentally, we have seen no difference between chains created by iodine and xenon ions.

2.2. Perpendicular incidence

A $SrTiO_3$ single crystal (Crystec, Berlin), cut along the (100)-plane, was irradiated under normal incidence with 92 MeV Xe^{23+} ions under a fluence of 2×10^{13} ions cm^{-2} at the IRRSUD beamline of GANIL (Caen, France). At these fluences, individual tracks overlap. After irradiation, the sample was cut and glued together with epoxy to produce two layers that are facing each other. This sandwich was then encased and glued in a 3 mm thin-walled tube. The tube was cut into 1 mm thick discs. These discs were mechanically thinned to about 100 μm in thickness and dimpled so that the centre thickness was less than 5 μm. Finally, Gatan's Precision Ion Milling System was used to thin the specimen from both sides with 3.5 keV Ar^+ ions at 5° incidence angle until perforation. These targets were studied with a 2010F Jeol transmission electron microscope equipped with a 200 keV field electron gun.

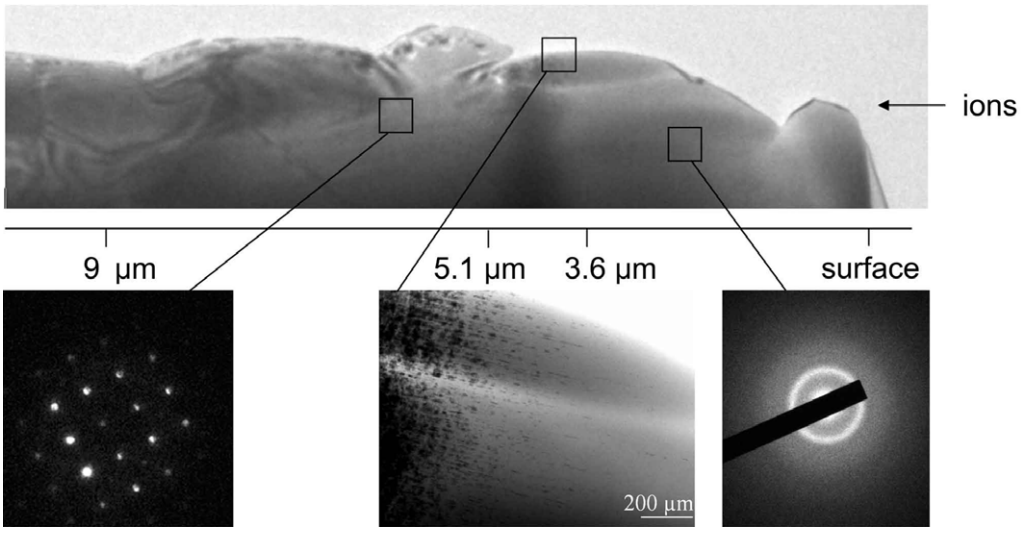

Figure 3. Upper part: TEM image of a $SrTiO_3$ sample irradiated under normal incidence. Ions enter on the right side: see arrow. The axis below the image shows the depth from the surface. Lower part: the central image is a magnification of the central part of the image on top. The left and right images in the lower part show the diffraction patterns obtained at ion penetration depths of 6 and 3 μm, respectively.

A TEM image of the obtained cross section is shown in the upper part of figure 3. The bright triangle on the right side stems from the glue, denoting the surface region of the crystal. The ions penetrate the crystal in the direction indicated by the arrow. In the first region along the trajectory, the crystal was amorphized by the projectile, as can be seen from the diffraction pattern on the right side, which was taken from this region of the crystal. This first region extends from the surface to a penetration depth of $\simeq$3.6 μm. To correlate these data with the stopping power, we performed SRIM calculations. The results are shown in figure 4. In the first region, where the crystal was amorphized, the electronic energy loss decreases from 21 to 11.7 keV nm^{-1}. From this, we determine the threshold of amorphization to be about 11.7 keV nm^{-1}.

At larger penetration depths, partial amorphization is seen in figure 3. This continues to a depth of 5.1 μm. At this depth, the energy loss is 7.3 keV nm^{-1}, according to SRIM, as shown in figure 4. At even larger penetration depths, the material remains single crystalline, as shown by the diffraction pattern on the left of figure 3. Therefore, we can distinguish two thresholds: one at 7.3 keV nm^{-1} for the appearance of partially amorphized tracks and one at 11.7 keV nm^{-1} for complete amorphization.

3. The two-temperature model

After we experimentally determined the minimum stopping power required to create a chain of nanodots, we focused on giving a theoretical description. Modifications to the standard TTM [9] were necessary because neither the variation in energy loss due to anisotropy of the electron density nor the close vicinity of the surface can be correctly described. Thus, in order to

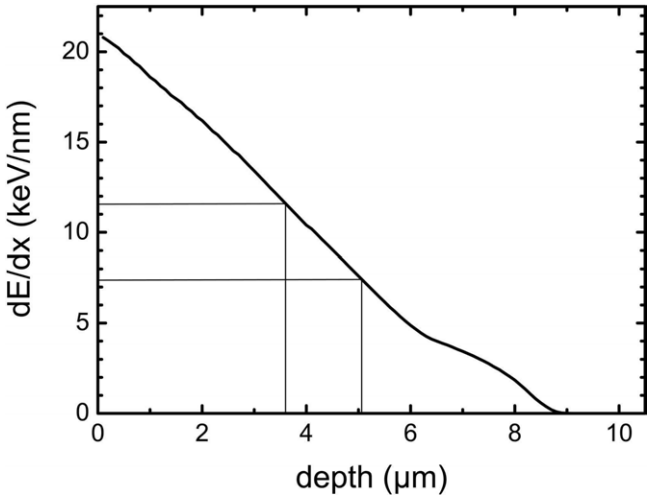

Figure 4. SRIM simulation of Xe ions impinging on a $SrTiO_3$ single crystal at 92 MeV kinetic energy. The electronic energy loss as a function of the penetration depth of the incident ion is shown. The thin lines denote the thresholds for complete amorphization and for the appearance of partially amorphized tracks, as determined from the TEM images of figure 3.

improve the TTM, we extended it to a full 3D description including the integration of a spatially resolved electron density [5, 14]. The general shortcomings of the TTM as e.g. discussed by Klaumünzer [6] are not solved by this approach. Unfortunately, there is still a lack of alternative theoretical models describing the hillock formation in detail. However, the modified TTM can be used in this paper because we are only interested in the threshold energy. The basic procedure for determining the threshold energy is described in detail in [14, 15] and will be explained here only insofar as it is necessary to understand the additions we have made to the model.

In order to determine the minimal necessary stopping power to create a *fully developed* chain, the following scheme was applied. The calculations were performed on the basis of a 3D TTM using space- and time-resolved electronic stopping powers for the actual case. It was proven before that there is a fixed maximum depth where it is possible for the incident ion to create surface hillocks due to the electronic energy loss [5, 14]. Therefore, the distance covered by the incident ion at the point perpendicular to the last hillock can easily be extracted using geometrical calculations from the incident angle and the above-mentioned maximum depth. The depth for $SrTiO_3$ is $d \simeq 8.5$ nm, and the track length l can then be calculated by $l = d \cot \phi$. In the next step, we calculated the energy loss of the ion at this precise point for different kinetic energies and used it as a source for the 3D TTM. In this way, surface temperatures at the end of the hillock chain could be obtained as a function of the incident ion energy: see figure 5. Assuming that the melting temperature ($T_{\mathrm{melt}} = 2353$ K [17]) has to be reached to induce surface modifications, the incident ion has to have a minimum kinetic energy of 31 MeV, corresponding to an energy loss of 12.7 keV nm^{-1}.

The calculation of the threshold for the *appearance* of chains in this way is much more difficult as the track length at stopping powers close to the threshold is no longer constant but depends on local fluctuations caused by impurities, defects, etc. This makes it necessary to solve the TTM equations at each point along the entire track of some hundreds of nm, including

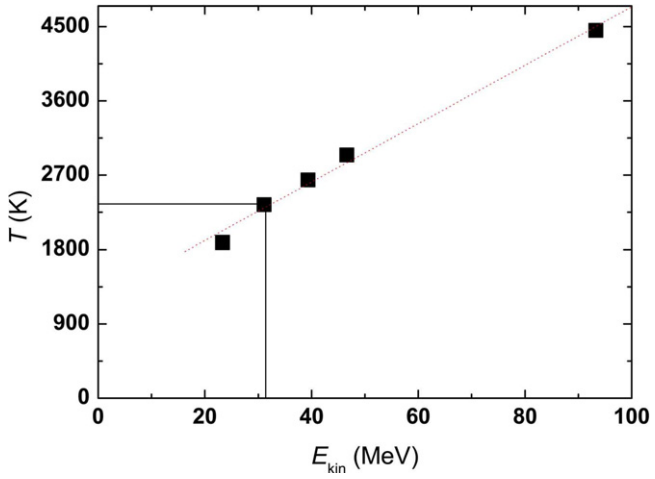

Figure 5. Temperature in K at the surface of $SrTiO_3$ when irradiated by Xe ions under different kinetic energies. To reach the melting temperature of $SrTiO_3$, the projectile has to have an energy of 31 MeV, corresponding to a stopping power of $dE/dx = 12.7\,\mathrm{keV\,nm^{-1}}$. The dotted line represents a linear fit to the data; it is given to serve as a guide to the eye.

fluctuations and repeating the calculations numerous times in order to account for the statistics. This leads to a tremendous increase of the computational effort. Instead we used the TTM to calculate the surface temperature that would result from ion irradiation under perpendicular incidence with stopping powers of 6, 7, 8 and 9 $\mathrm{keV\,nm^{-1}}$. The resulting temperatures were 1830, 2100, 2350 and 2580 K, respectively. These values indicate that the lower threshold should be approximately 8 $\mathrm{keV\,nm^{-1}}$, which is in good agreement with the experimental data.

All calculations ignore the necessary (but unknown) heat of fusion, and the energy loss values obtained in this way therefore present a lower limit. Additionally, the model calculations were performed for Xe ions. The minimum kinetic energy for I ions would have to be only slightly higher to achieve the same stopping power.

4. Discussion

In table 1, all the threshold values obtained for glancing and normal incidence, as well as the theoretical predictions, are shown. Experimental and theoretical data indicate that two threshold values exist.

If the energy loss is lower than $\simeq$7 $\mathrm{keV\,nm^{-1}}$ the energy stored in the electronic system is simply not sufficient to melt the material and no modifications are observed. This first threshold should therefore be comparable to the minimum energy loss that is necessary to produce a nanodot on the surface irradiated under perpendicular incidence (see section 3). Under glancing angles, tracks appear at kinetic energy losses larger than (5.3–7.2) $\mathrm{keV\,nm^{-1}}$ when studied by means of AFM (section 2.1). The tracks are shorter because the energy loss is close to the threshold for melting and will easily fall below the critical value due to fluctuations, resulting in a missing hillock or an incomplete track, respectively. This fits well with the TEM measurements (section 2.2), where the appearance of tracks was seen for energy losses of 7.3 $\mathrm{keV\,nm^{-1}}$. The

Table 1. Threshold values in keV nm^{-1} obtained from the experiments (AFM and TEM) and the TTM.

Grazing angle (AFM)	Appearance of chains 5.3–7.2	Constant length of chains 10.5–21
Normal incidence (TEM)	Appearance of tracks 7.3	Amorphization 11.7
Grazing angle (TTM)		Constant length of chains 12.7
Normal incidence (TTM)	$T \geqslant T_{\mathrm{melt}}$ 8	

TEM measurements show discontinuous tracks at these low energy loss values, in agreement with the AFM data.

Amorphization in the bulk (TEM), as well as fully developed surface tracks (AFM), can only be seen at energy losses above 11.7 keV nm^{-1} and (10.5–21) keV nm^{-1}, respectively. This second threshold fits well with the calculated threshold of 12.7 keV nm^{-1}, where melting of the surface over the full surface track length was defined as a requirement to produce hillocks (see section 3). If the energy loss approaches the threshold, the remaining energy loss at the maximum depth d may not be sufficient to result in surface modifications. For sufficiently high energy losses, d is constant even if the initial energy loss of the impinging ion changes by over 70% [16]. This can explain why surface track length increases with increasing energy loss as observed in figure 2.

The discovery of two different values for the hillock creation is not a contradiction: it merely reflects that the hillock creation at stopping powers $\geqslant$12.7 keV nm^{-1} is independent of statistical fluctuations. Below this value, the individual nanodot creation is a more statistical phenomenon, which results in 'incomplete' tracks.

5. Conclusion

We have presented new experimental AFM and TEM data from which two thresholds for the formation of ion tracks in $SrTiO_3$ were established, one for the formation of surface tracks and the other for distinguishing between partially and fully developed (i.e. full length) surface tracks. These findings are in agreement with calculations based on the TTM. The determination of the threshold with surface tracks has two main advantages. Experiments performed under perpendicular incidence create single hillocks, which are difficult to identify in *ex situ* experiments, especially if the production efficiency goes down or the single hillocks become smaller as they approach the threshold. A chain is easily spotted and can be unambiguously identified as an ion-induced feature, for example the direction must comply with the direction of the irradiation. Because we made no specific assumptions with respect to the material, we believe that the method is capable of predicting the minimal energy required to create nanodots in many other insulating materials of technological importance, such as Al_2O_3 or TiO_2.

Acknowledgments

We thank R Meyer for calculating the electron density and for stimulating discussions. The financial support of the DFG through SFB 616: *Energy dissipation at surfaces* and the International Atomic Energy Agency (IAEA) through the research project CRO12925 is gratefully acknowledged. Experiments were performed at the Institut Ruder Bošković and GANIL (Caen, France).

References

[1] Müller A, Neumann R, Schwartz K and Trautmann C 1998 Scanning force microscopy of heavy-ion tracks in lithium fluoride *Nucl. Instrum. Methods* B **146** 393

[2] El-Said A S, Cranney M, Ishikawa N, Iwase A, Neumann R, Schwartz K, Toulemonde M and Trautmann C 2004 Study of heavy-ion induced modifications in BaF_2 and LaF_3 single crystals *Nucl. Instrum. Methods* B **218** 492

[3] Awazu K, Wang X, Fujimaki M, Komatsubara T, Ikeda T and Ohki Y 2006 Structure of latent tracks in rutile single crystal of titanium dioxide induced by swift heavy ions *J. Appl. Phys.* **100** 044308

[4] Khalfaoui N, Görlich M, Müller C, Schleberger M and Lebius H 2006 Latent tracks in CaF_2 studied with atomic force microscopy in air and in vacuum *Nucl. Instrum. Methods* B **245** 246

[5] Akcöltekin E, Peters T, Meyer R, Duvenbeck A, Klusmann M, Monnet I, Lebius H and Schleberger M 2007 Creation of multiple nanodots by single ions *Nat. Nanotechnol.* **2** 290

[6] Klaumünzer S 2006 Thermal-spike models for ion track physics: a critical examination *Mat. Fys. Medd. Dan. Vid. Selsk.* **52** 293

[7] Schiwietz G, Xiao G, Luderer E and Grande P L 2000 Auger electrons from ion tracks *Nucl. Instrum. Methods* B **164** 353

[8] Toulemonde M, Dufour C and Paumier E 2006 The ion–matter interaction with swift heavy ions in the light of inelastic thermal spike model *Acta Phys. Pol.* A **109** 311

[9] Toulemonde M, Dufour C and Paumier E 1992 Transient thermal-process after a high-energy heavy-ion irradiation of amorphous metals and semiconductors *Phys. Rev.* B **46** 14362

[10] Jaksic M *et al* 2007 New capabilities of the Zagreb ion microbeam system *Nucl. Instrum. Methods* B **260** 114

[11] Ziegler J F and Biersack J P 2008 *The stopping and range of ions in matter (SRIM)* http://www.srim.org

[12] Horcas I, Fernandez R, Gomez-Rodriguez J M, Colchero J, Gomez-Herrero J and Baro A M 2007 *Rev. Sci. Instrum.* **78** 013705

[13] Akcöltekin S, Akcöltekin E, Roll T, Lebius H and Schleberger M 2009 Patterning of insulating surfaces by electronic excitation *Nucl. Instrum. Methods* B **267** 1386

[14] Akcöltekin E, Akcöltekin S, Osmani O, Duvenbeck A, Lebius H and Schleberger M 2008 Swift heavy ion irradiation of $SrTiO_3$ under grazing incidence *New J. Phys.* **10** 053007

[15] Osmani O, Duvenbeck A, Akcöltekin E, Meyer R, Lebius H and Schleberger M 2008 Calculation of electronic stopping power along glancing swift heavy ion tracks in perovskites using *ab initio* electron density *J. Phys.: Condens. Matter* **20** 315001

[16] Akcöltekin S, Akcöltekin E, Schleberger M and Lebius H 2009 Scanning probe microscopy investigation of nanostructured surfaces induced by swift heavy ions *J. Vac. Sci. Tech.* B **27** 944

[17] Dittrich H, Karl N, Kück S, Schock H W and Madelung O 2000 *Semiconductors: Ternary Compounds, Organic Semiconductors* (*Landolt–Börnstein Group—Condensed III Matter* vol 41E) (Berlin: Springer)